Journal of Applied Fluid Mechanics, Vol. 7, No. 1, pp. 75-87, 2014.
Available online at www.jafmonline.net, ISSN 1735-3572, EISSN 1735-3645.

Parametric Study of Exhaust Pattern in Cold Spray Using CFD and Particle-Wall Impact Analysis

M. Karimi†, G. W. Rankin and A. Fartaj

University of Windsor, 401 Sunset Avenue, Windsor N9B 3P4, Ontario, Canada

†Corresponding Author Email: *karimi1@uwindsor.ca*

(Received October 15, 2012; accepted February 6, 2013)

ABSTRACT

A numerical simulation of a cold gas dynamic spray process using a computational fluid dynamic (CFD) technique is presented. Distribution of particulate matter in the immediate surroundings of spray application site is of interest. The flow field inside an oval shaped supersonic nozzle and the surroundings of the nozzle is simulated. Particle trajectories along their flight in the nozzle as well as before and after impact with the target plane are calculated. Fluent is used for the purpose of flow field simulation. A discrete-phase Lagrangian particle trajectory model is used for particle trajectory calculation. A model uses the principles of motion and impact dynamics to predict particle behavior upon impacting the substrate. The locations and concentrations of particle exhaust patterns around the impact location are determined and presented graphically. The dependence of these patterns to variations in the jet-target tilting angle, standoff distance, upstream temperature and particle material is investigated.

Keywords: Cold spray, Numerical simulation, Discrete phase modeling, Particle distribution.

NOMENCLATURE

C_D	drag coefficient
d	diameter
e	coefficient of restitution
f	friction factor
h_e	elastic recovery
h_p	depth of impact crater in target
l	standoff distance
M	rotational mechanical impulse
Nu	Nusselt number
o	stagnation
p	pressure
P	linear mechanical impulse
p	Particle
r	particle radius
s	substrate
t	tangential component of vector
t	maximum nozzle thickness
T	temperature
v	velocity prior to impact
V	velocity after impact
w	domain semi-width
y	target center to boundary clearance
z	distance along nozzle axis from nozzle throat
Subscripts	
e	nozzle exit
f	particle-feed
m	melting point
n	normal component of vector
Superscript	
*	nozzle throat
ε	dynamic hardness
θ	angle between target normal and nozzle axis
μ	mechanical impulse ratio
ρ	Density
σ_T	tensile strength
Ω	angular velocity

1. INTRODUCTION

Kinetic Spray processes are methods of applying coatings of powdered materials through impinging them on a substrate (Karimi *et al.*, 2011) at very high speed, relying mainly on the kinetic energy of the particles as opposed to their thermal energy to create the bond.

The Cold Spray (Cold Gas Dynamic Spray, or CGDS) process belongs to the Kinetic Spray family of coating processes. Due to the low temperatures used in the process, when compared to other variations of Thermal Spray processes, cold spray offers many advantages (Alkhimov *et al.*, 1990, 1994, 1995).

In this process powder particles are entrained into a gas stream and accelerated to supersonic speeds using a carrier gas passing through a converging-diverging, or DeLaval, nozzle. Depending on the specific equipment type, particles can be introduced upstream or downstream of the throat. Introducing particles downstream of the throat will simplify the powder feeding mechanism and is considered in this paper (Kashirin *et al.*, 2002). The nozzle geometry and gas supply pressure can be designed such that the pressure at the particle feed is lower than the ambient pressure. Under these conditions the powder particles are drawn into the main gas stream. As a result the powder feeding mechanism can be very simple allowing for the packaging of the equipment into a portable device.

Generally, using this process causes some particles to achieve energy levels required to create a bond with the substrate. Depending on the type of material and distribution in size of the sprayed particles, some will rebound and remain in the surroundings. This is the source of different levels of health and safety hazards (Clift *et al.*, 1978; Konstandopoulos 2006). To minimize possible risks, a common practice is to use a dedicated spray booth or ventilation unit for the purpose of conducting the spray work. This negates the portability of the equipment making it unsuitable for applications where utilizing a ventilation system is not possible. A possible approach to addressing this issue is to design a portable exhaust collection system.

The ability to design such a capture-at-source particle exhaust system requires an understanding of the flow field as well as the trajectories of the particles. Methods of modeling kinetic spraying processes, including both gas and particle flow, are developed and published in the literature (Dykhuizen and Smith, 1998; Grujicic *et al.*, 2003; Jodoin, 2002; Karimi *et al.*, 2011; Stoltenhoff *et al.*, 2002). In these models, however, the objective is to investigate the performance of the process, hence modeling usually stops where particles reach the substrate. A model was previously developed to investigate the interaction of particle and the substrate in order to enable prediction of particle behavior after impacting on, and bouncing off the substrate (Karimi *et al.*, 2006). In this case the particle impact model is combined with other Computational Fluid Dynamics (CFD) tools to predict particle behavior and distribution around the nozzle exit. The locations of particles leaving a surface of interest, and their concentration levels around these locations are presented in a useful graphical manner.

This paper is a follow-up to the previous paper (Karimi *et al.*, 2006). It presents the details and recent advancements to the particle-wall impact model, which was not included in the original paper. Therefore the details of the model concerning the gas flow field are not included. This paper presents an application of the model to various cases in order to guide the design of a capture-at-source exhaust system. The objective of the work is to investigate the effect of change in the nozzle-target standoff distance (l,) relative angle between the nozzle axis and the target normal (θ,) upstream temperature (T_o) and particle material as represented by its density (ρ_p.)

2. NUMERICAL METHODOLOGY

Parts of the information in this section pertaining to calculations of the fluid phase appear, in a relatively concise (Karimi *et al.*, 2006) or thorough manner (Karimi, 2005), in the available literature and are presented here in summary form to best serve the purpose of this article. The portions relating to particle trajectory predictions are emphasized here.

For simulation purposes, FLUENT 6.2 (Ansys Inc., Lebanon, NH, USA) is used. The geometrical domain used for the calculation, as well as the geometry and mesh for one typical set of parameters is shown in Figure 1. Values of 2 cm and 2.5 cm for the distances y and w are large enough for this simulation. They allow capturing all the important flow features and giving an accurate description of the distribution of particles that leave the enclosure. The boundaries are confirmed to be placed far enough away such that this distance does not affect the numerical solution of the flow.

The nozzle tube has a circular cross-section upstream of the particle feed location. The diameter of the throat, d*, is 2.66 mm. This circular shape is transformed smoothly into an oval shape in the diverging tube which starts downstream of the particle feed, and extends to the exit of the nozzle. The nozzle has a length of approximately 12 cm with cross-sectional dimensions at its exit plane, t_e, have values of 9.0 mm for the major axis, and 6.0 mm for the minor axis, respectively. Distances of the exit plane of the nozzle tube , and particle feed, from the throat of the nozzle, are denoted z_e and z_f. The values of these dimensions are 13.9 cm for z_e and 5.6 mm for z_f respectively. These geometrical properties pertain to cold spray systems available from CenterLine (Windsor) Limited, one of the most prominent manufacturers of cold spray equipment especially portable systems.

2.1 Flow Field

A structured grid scheme is implemented using hexahedral elements everywhere except near the nozzle axis. Adjacent to this axis wedge elements are required (See Fig. 1). The mesh has 29,760 cells inside the nozzle. The environment region has between 53,166 and 94,042 cells. This variation is due to variations in the target tilting angle, θ, and the standoff distance, l. The independence of the result to grid size is checked using a grid dependency study (Karimi, 2005).

The continuity, momentum and energy equations are used along with the ideal-gas law to account for

compressibility effects. A modification to the k-ε model which accounts for compressibility effects is used to model the turbulence. This method was suggested and successfully used by Sarkar *et al.* (1991) and Sarkar and Lakshmanan (1991). In addition, the dependence of viscosity on temperature is included by using the Sutherland law which is suited for high-speed compressible flows (Fluent Inc., 2011). A coupled-implicit solver is used for this study with a discretization scheme of second order (Karimi, 2003; Fluent Inc., 2011).

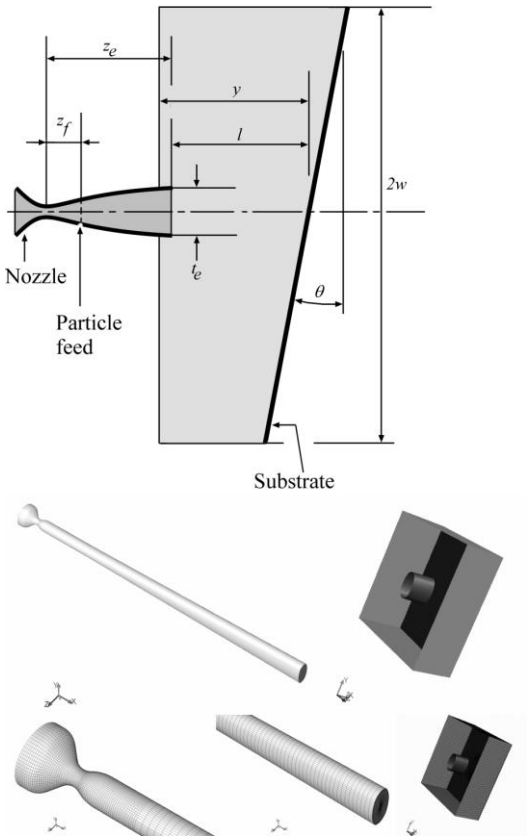

Fig. 1. Calculation domain for the simulation (not to scale.)

2.2 Particle-Fluid Interaction

Particle trajectory calculations are conducted using a Lagrangian reference frame. This is based on the assumption that the particulate phase is sufficiently dilute to neglect particle-particle interactions as well as the effects on the gas phase of particle volume fraction. The discrete phase, therefore, must exist at low volume fractions, which is known to be the case (Dykhuizen and Smith, 1998; Karimi, 2005; Shipway and Hutchings, 1994; Shukla *et al.*, 2000).

Particle motion is caused by the drag force that is applied on the particles by the adjacent flow field. The force magnitude depends on the drag coefficient, denoted by C_D. A correlation proposed by Clift *et al.* (1978) accounts for a large range of relative flow-particle conditions. This correlation is general enough to cover the conditions encountered in the problem in hand. It is incorporated in the solver as the high-Mach-number Drag Law and is used directly in this simulation.

The stochastic nature of the turbulence in the flow affects the particle trajectories. A Stochastic Tracking technique, available as an option in the solver, is used to model the dispersion of particles due to turbulence (Tannehill *et al.*, 1997). The technique estimates the instantaneous fluid velocity at each point along the path of integration.

The transfer of heat between the particle and the carrier gas is very important as some characteristics of the impact phenomenon depend on the temperature of particle at the time of impact (Kosarev *et al.*, 2003; Schmidt *et al.*, 2006). Due to the very small size of particles it can be assumed that they have negligible internal resistance to heat transfer and therefore remain at uniform temperature throughout (previously demonstrated by Stoltenhoff *et al.* (2006). In order to predict heat transfer to particles, the value of Nu_p (flow-particle Nusselt number) is used. This represents the convective to conductive heat transfer ratio, in non-dimensional form. A correlation is used in this study that depends on the speeds and other known heat transfer properties of the gas and particle phases. It has been shown that this correlation accurately predicts the temperature values of particles. This is the default correlation incorporated in the solver and is used for this study.

2.3 Particle-Wall Interaction

Generally, when a particle hits a surface, it either sticks to it or bounces off. This sticking phenomenon can be of two types, adhesion or bonding. In the case of adhesion, commonly studied for pollen and spores, there is no structural bond between the particle and the surface. Various aspects of this phenomenon have been examined by many researchers (Konstandopoulos, 2006; Walter, 1995), mainly for applications concerning dust collection techniques. In the CGDS application, however, the nature of the sticking phenomenon is attributed to local structural bonding between the particles and the substrate (Schmidt *et al.*, 2006). In such cases, whether the particle bonds to the surface or not depends on several parameters including particle kinetic energy, impact temperature, its shape, size, as well as the angle of attack (Gilmore *et al.*, 1999; Schmidt *et al.*, 2006; Van Steenkiste *et al.*, 2002). In order to determine whether a particle bonds to the surface or rebounds, the normal component of impact velocity should be higher than a characteristic velocity called the critical velocity.

Bonding in cold spraying is associated with localized deformation of participating bodies as well as shear instabilities. Critical velocity is the velocity at which these phenomena start to occur under a specific set of impact conditions. In predicting particle trajectory

pursuant to impact upon the substrate, it is first determined if it will bond or rebound using critical velocity information as the determining criterion. For this purpose an equation proposed in the literature (Schmidt *et al.*, 2006) is utilized resulting in critical velocity values in the range of 440-480m/s for copper particles and 590-640m/s for aluminum particles (Schmidt *et al.*, 2006) considered in this study.

Trajectory tracking for particles that deposit on the surface is terminated. For the rebound case, the impact dynamics equations are considered in order to estimate the normal and tangential particle velocity components after impact. The equations for a sphere travelling on a plane that is perpendicular to the plane of target involve the equations of normal, tangential and angular momentum denoted by P_n, P_t and M respectively in Fig.2 (Brach, 1988). An angular velocity is not considered for particles, however, the equations of angular momentum are retained in the impact analysis. The initial particle angular velocity upon impact with the wall is assumed zero. Its updated value is ultimately discarded upon the completion of the calculations of impact.

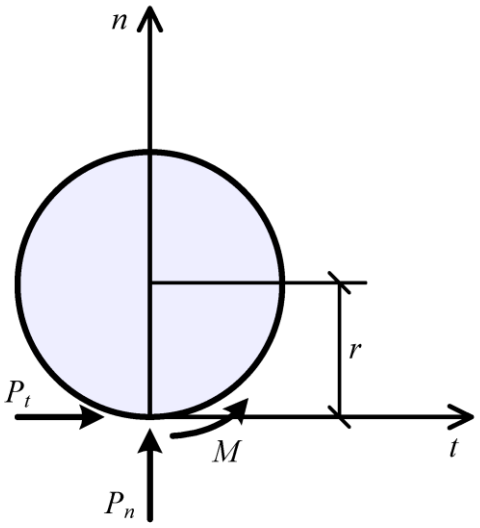

Fig. 2. Free body diagram of a sphere impacting on a surface

Upon impact, the particle begins to slide on the surface. Two different scenarios can occur depending on the impact conditions. In determining which scenario will take place, the values of the coefficient of friction, f, and the impulse ratio, μ, defined by Eq. (1) (Brach, 1988) play major roles.

$$\mu = \frac{P_t}{P_n} = \frac{V_t - v_t}{V_n - v_n} \tag{1}$$

In the first scenario, a particle continues to slide throughout the impact. The impact dynamics equations in this case are given by Eq. (2) through Eq. (4) (e_n is the normal coefficient of restitution, r is the particle radius) (Brach, 1988). These equations determine the normal, tangential and angular velocity components after impact (capital letters), in terms of those before impact (small letters).

$$V_n = -e_n v_n \tag{2}$$

$$V_t = v_t - \mu(1+e_n)v_n \tag{3}$$

$$\Omega = \frac{5}{2r}\mu(1+e_n)v_n \tag{4}$$

In the second scenario, the sliding motion ends prior to the end of the contact. After sliding is finished, the particle begins to roll, and this will continue until the end of contact. With this scenario, velocity components after the contact relate to those before the contact as described by Eq. (5) through Eq. (7) (Brach, 1988).

$$V_n = -e_n v_n \tag{5}$$

$$V_t = \frac{5}{7}v_t \tag{6}$$

$$\Omega = \frac{5}{7r}v_t \tag{7}$$

In order to determine the appropriate set of equations, one must determine which scenario takes place in a given situation. According to Brach (1988), if the coefficient of friction, f, is relatively small, say f_1, the tangential impulse $P_t = f_1 \bullet P_n$ will be insufficient to cause sliding to end prior to separation. As f increases, it reaches a critical value, say f_2, just large enough to cause sliding to end at the time of separation. For any value of f larger than this critical value, the impulse necessary to cause sliding to cease occurs earlier in time. At that time, rolling begins and the tangential force drops to some relatively small value. Consequently, part of the contact duration contains sliding and the remainder rolling. For all coefficients of friction which are greater than f_2, the tangential impulse will never exceed $f_2 \bullet P_n$. Thus a limiting critical value of impulse ratio μ exists and is denoted by μ_c. Under no condition can the value of the tangential impulse exceed $\mu_c \bullet P_n$. The limiting condition occurs when the solution equations for sliding are identical to the solution equations for rolling, resulting in μ_c as given by Eq. (8).

$$\mu_c = \frac{2}{7}\frac{v_t / v_n}{(1+e_n)} \tag{8}$$

Briefly, in order to determine the correct scenario, f should be compared with the value of μ_c given by Eq. (8). If f is smaller than this critical value, the first scenario occurs, and therefore Eq. (2) through Eq. (4) should be used. Otherwise, Eq. (5) through Eq. (7) will be the proper choice.

Conditions in CGDS applications are such that particle trajectories are nearly axial leaving the nozzle. The maximum deviation of trajectories from the axial direction is the angle of the nozzle wall, in the case of

this study less than 1 degree. Therefore the maximum angle between this particle track upon impact and substrate normal is dominated by the angle of spray application from the substrate normal that has a maximum value of 10 degrees in this study, resulting in a maximum overall impact angle of 11 degrees. Under such a condition, regardless of the value of the normal coefficient of restitution, the critical impulse ratio is always smaller than 0.05 (Eq. (8)). This is smaller than the f value normally encountered in metal-metal contacts, which is generally greater than 0.1. Therefore, the latter scenario always occurs resulting in a value of 5/7 for e_t, the tangential coefficient of restitution.

A procedure proposed by Kleis and Hussainova (1999) is used to estimate e_n, the normal coefficient of restitution. This procedure relies on the energetic impact theory and takes into consideration the mechanical properties of the substrate and the impacting particle. In this procedure the normal coefficient of restitution is calculated based on Eq. (9). In this equation h_e is the elastic recovery, or the total elastic deformation of the particle and target in normal direction, and h_p is the depth of impact crater in target surface.

$$e_n = \sqrt{\frac{4}{5}\frac{h_e}{h_e + h_p}} \tag{9}$$

The value of h_p can be found, based on energetic theory of impact, from Eq. (10). In this equation ε_s represents the dynamic hardness of the substrate. This value is cited for a few materials by Kleis and Hussainova (1999). For copper, the substrate material under consideration in this study, the value of dynamic hardness is 1.7×109 J/m^3. In addition to material properties, h_p is evidently a function of impact conditions. Elastic recovery, h_e, on the other hand, is only a function of material properties of both the substrate and the impacting particle (Kleis and Hussainova, 1999).

$$h_p = vr\sqrt{\frac{2}{3}\frac{\rho_p}{\varepsilon_s}}, \qquad h_p + h_e \le 0.2r$$

$$h_p = r - 2r\cos\left\{\frac{1}{3}\arccos\left(1 - \frac{\rho_p v^2}{\varepsilon_s}\right) + \frac{\pi}{3}\right\} \tag{10}$$

$$, \qquad h_p + h_e > 0.2r$$

One can see that, based on Eq. (9), if the normal coefficient of restitution, e_n, is known at one arbitrary velocity, with the knowledge of other material properties the value of elastic recovery can be estimated. For the impact of aluminum and copper spheres of the size range of interest this information is not available in the literature. For a known impact of hardened steel balls on a steel-30 substrate (Kleis and Hussainova, 1999) the value of normal coefficient of restitution at just below critical velocity is 0.06. It is assumed here that normal coefficient of restitution for the impacts of interest also take a value of 0.06 at just below critical velocity. This is expected to be a good assumption as it is known (Assadi *et al.*, 2011) that many aspects of impact (both erosive and adhesive properties such as resulting deposition efficiency and bond strength) are common among various situations when velocity is non-dimensionalized with respect to critical velocity.

The material properties for these impacts are listed in Table1, along with calculated values of elastic recovery. All of the properties were found from Matweb (2012) except for the dynamic hardness which was found in Van Steenkiste *et al.* (2002). Calculations for elastic recovery are performed for a typical 30-micron particle. Under these impact conditions critical velocities are estimated to be 458 m/s and 608 m/s for copper and aluminum particles respectively (Schmidt *et al.*, 2006).

Using this approach the value of normal coefficient of restitution as a function of impact speed for the material combinations of interest, namely aluminum and copper on a copper substrate, are calculated and plotted in Fig.3 (a). For the sake of comparison, the coefficient of restitution for the impact of hardened steel on steel substrate is also plotted in Fig. 3 (b). Evidently, the predicted coefficients of restitution exhibit a very similar trend to that of the known impact. These calculations are incorporated in the solver using a User-Defined Function (UDF).

Table 1 Material properties used for calculating normal coefficients of restitution

Particle				**Substrate**		
Material	**Density, ρ_p kg/m^3**	**Melting Temperature, $T_{m,p}$ K**	**Tensile Strength, $\sigma_{T,p}$ MPa**	**Material**	**Dynamic Hardness, ε_s×10^{-9} J/m^3**	**Elastic Recovery, h_e microns**
Aluminum	2699	933	160	Copper	1.7	0.05
Copper	8930	1357	210	Copper	1.7	0.078

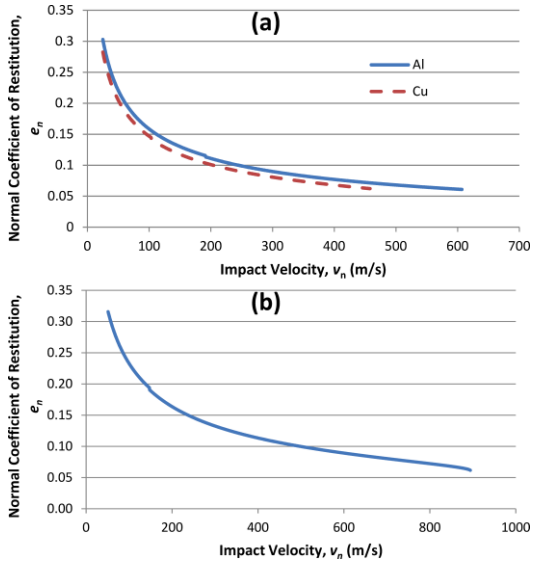

Fig. 3. (a) Calculated values of normal coefficient of restitution as a function of impact velocity for 30-micron aluminum and copper particles, (b) Normal coefficient of restitution as a function of impact velocity for 1.6-mm hardened steel particles.

2.4 Boundary and Initial Conditions

2.4.1 Flow Field

At the nozzle inlet, a pressure inlet boundary condition is assigned using values of static pressure, p, measured using a pressure gauge located upstream of the nozzle throat. Total temperature, T_o, is found using a thermocouple. The total pressure, p_o, is taken as being equal to the static pressure due to the very low velocity at this section. A length scale value of one-fifth of the nozzle diameter and turbulence intensity value of 1% and are assumed at the inlet which have been shown previously to be appropriate for similar flow fields (Karimi *et al.*, 2005).

The boundaries surrounding the environment are pressure outlets, with a pressure value equal to the atmospheric pressure. In these regions, the velocity vector direction is matched with neighboring cells. All walls are treated as a standard wall boundary condition. This enforces a zero-velocity of the gas at the wall location.

2.4.2 Particle Tracking

The nozzle region contains a particle feed section. The particle feed tube is at a 45° angle with the nozzle tube. The projection of the particle feed tube cross-section on the cross-section plane of the nozzle shapes an ellipse. In the numerical model particles are randomly distributed on this ellipse and initiated from this site. The distribution is weighted such that the chances are greater of particles appearing closer to the particle feed tube center than its periphery, as expected to be the case in reality.

2.5 Numerical Experiment

The numerical methodology that has been developed is used to investigate the effect of changes in certain parameters on the particle trajectories. These parameters and the range of their variations are summarized in Table2. Combination of these parameters results in 36 different cases which are considered in this study.

Table 2 Parameters considered and their values

Parameter \ Value	**1**	**2**	**3**
Standoff Distance l (mm)	5	10	15
Target Tilting Angle θ (degrees)	0	5	10
Upstream Temperature T_o (°C)	100	300	N/A
Particle Material [Density, ρ_p (kg/m^3)]	Al [2719]	Cu [8978]	N/A

In all cases the value of total pressure, p_o, is 72 psig (500 kPa gauge). This pressure value is available in most machine shops and is typical of spraying condition using a low-pressure cold spray machine. The particle size range used in this simulation is 25 to 38 microns, typical of particle size range used in cold spraying. A low temperature value, namely 100 °C, and a higher temperature of 300 °C is considered in order to understand effect of process temperature. The higher temperature is close to the temperature used for actual spray applications using both aluminum and copper materials (usually in the range of 300-350 °C).

3. RESULTS

3.1 Model Validation

The model is validated for both fluid phase as well as discrete phase calculations. Details of this validation have previously been published in the literature (Karimi, 2005, Karimi *et al.*, 2006). Experimental values of wall pressure along the nozzle tube are used for validating the fluid phase calculation for the cases of 100 °C and 300 °C upstream temperatures. Particle velocities at the exit plane of the nozzle are used for validating particle trajectory calculations.

3.2 Presentation of Results

An investigation of a generic case showed that a statistically large enough sample for the results to be independent of particle count is would contain 7000 particles. This number is used in obtaining the following images. The trajectories are contained in a FLUENT output file, which includes the data extracted from all particle properties, and recorded at each time step. A computer code in C-language is created to process the data contained in this file. A MATLAB program is developed to generate contours of concentration of particle crossing a surface of interest. For ease of visual interpretation a hemispherical shape is used as the surface of interest. This allows for comparison of concentration levels of particles at

equal distances from the central point of the substrate (where the jet lands on the target) regardless of the direction of particle motion. The results are universally normalized among all the images such that the same color shade would represent the same particle concentration in all images. The white regions have no particle passing through them. Even if a single particle passes through a region, a small region of a dark shade is created.

An image that represents the case of l = 10 mm, θ = 5 degrees, To = 300 °C and aluminum particles is shown in Fig.4 for the purpose of this discussion. The center of this hemisphere is located where the centerline of the nozzle intersects the target plane. This is always at an x and y co-ordinate of 0 mm, and a z co-ordinate of -10 mm. With a stand-off distance of 10 mm, the center of the exit plane of the nozzle falls on the z co-ordinate of 0 mm. The hemisphere has a radius of 20 mm. The black rectangle that is shown at the center of the top view represents the intersection of the nozzle tube with this imaginary hemispherical surface.

From the top view it is evident that this rectangle is not aligned with the pole of the sphere. This is due to the fact that the target substrate is tilted with respect to the nozzle tube by a particular angle (5 degrees in this case)

Clearly most particles leave the sphere through a band which starts from one side of the nozzle and extends to the target plane. Particle concentration levels within this band are significantly higher closer to the nozzle side, which forms a bright spot in that region. Under the conditions of this case, the tilting direction of the target plays a large role in the direction and location of the particle trajectories after they rebound from the target. The shape of high-concentration band is not symmetric about the plane of symmetry of the nozzle tube. This is attributed to the asymmetric location of the particle entrance in the nozzle tube.

3.3 Parametric Study

There are many important aspects regarding the performance of a spray process. An important example is the ratio of adhering particles to impacting particles, commonly referred to as Deposition Efficiency (DE). These aspects however, have been extensively studied elsewhere, and are not of interest in the current work. The purpose of this study is to analyze the pattern of the exhaust dust particle motion entering the surrounding ambient air relevant to the design of a capture-at-source exhaust device. In fact, in this study the spray conditions are such that particles in all cases do not adhere to the surface. This condition is chosen as it represents a worst-case scenario for dust entrainment in the surrounding ambient.

The effect of each parameter on the exhaust pattern is investigated separately. The exhaust patterns demonstrate three important characteristics to be considered. In most images, a high-intensity concentrated region, within the low-density darker region, can be distinguished. The location of this region is the first characteristic of interest. The location of the center of the spot (the whole colored region) is the second one. Finally, the size of the spot is considered. All the analyses are performed qualitatively and relative to one another.

3.3.1 Target Tilting Angle

In order to investigate the effect of target tilting angle, the cases similar to that shown in Fig. 4 but with tilting angles of 0 and 10 degrees are chosen and shown in Fig. 5 and Fig. 6. In the case of zero-degree target tilting angle, the particles spread in an approximately equal manner over the environment and exhibit no particular preferential direction (except a slightly higher intensity towards the right side of the domain due to the particle feed orientation.) As the angle increases, the high-intensity point and a clear spot start to form. At a 5-degree angle, the high-intensity point is located very close to the nozzle. The spot spreads in a band from the nozzle wall to the target towards the tilting angle. The location of the center of this region, therefore, is half way between the nozzle wall and the target. At the largest angle (10 degrees,) most of the particles are located around the high-intensity point. The location of the high-intensity point does not change in this case, but the spot spreads mostly around this point. The location of the center of this spot, therefore, is closer to the nozzle wall than the target.

Similar trends can be observed in all other cases investigated. In cases of shortest (5-mm) standoff distance, a clearer spot tends to form between the high-intensity point and the target. This is likely due to the reflection of some particles from the edge of the nozzle, which does not occur in larger standoff distances. In these cases, the size of the spot is larger and the location of its center is closer to the target.

3.3.2 Standoff Distance

The cases similar to that shown in Fig. 4 but with standoff distances of 5 mm and 15 mm are chosen and shown in Fig. 7 and Fig. 8 respectively. In all cases, the high-intensity point is located very close to the nozzle. This point cannot be easily distinguished in the closest distance. The spot spreads in a band from the nozzle wall to the target towards the low end of the target in all cases, with a fairly similar size. The location of the center of this region, therefore, is approximately half way between the nozzle wall and the target.

Similar trends can be observed in all other cases. In cases of zero-degree target tilting angle, the trend cannot be observed because the particles spread in an approximately equal manner over the environment and exhibit no particular distribution. In the case of largest (10-degree) target tilting angle, the pattern is mostly concentrated around the high-intensity point and the spot does not spread closer to the wall as much.

3.3.3 Upstream Temperature

The one case similar to that shown in Fig. 4 but with the upstream temperature of 100 °C is chosen and shown in Fig. 9. The location of the high-intensity

point and the center of the spot are not affected by upstream temperature. At the higher temperature, however, the particles tend to spread slightly more in space and the spot becomes slightly larger. In the case of zero-degree target tilting angle, the trend cannot be observed because the particles spread in an approximately equal manner over the environment.

3.3.4 Particle Material

The one case similar to that shown in Fig. 4 but with copper particles is chosen and shown in Fig. 10. The location of the high-intensity point and the center of the spot do not change with the particle material. In case of aluminum, the particles tend to spread significantly more in the space than copper, and therefore the spot becomes significantly larger. This can be associated with the lower density of aluminum which causes aluminum particles to be more easily influenced by turbulence and hence follow a more random trajectory. Even in cases of zero-degree target tilting angle, the space is completely filled in the case of aluminum particles, whereas some clean regions can be identified in the case of copper particles.

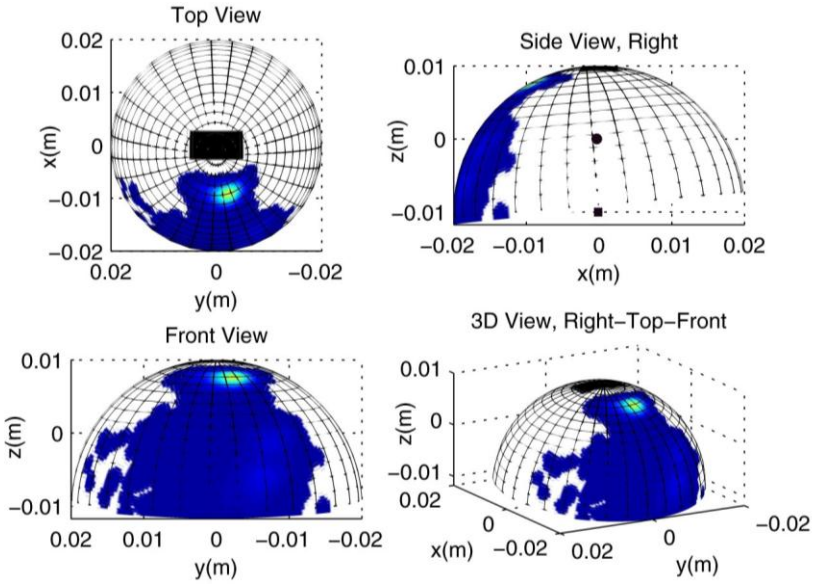

Fig. 4. Concentration of Al particles entering the surrounding; l = 10 mm, θ = 5 degrees, T_o = 300 °C.

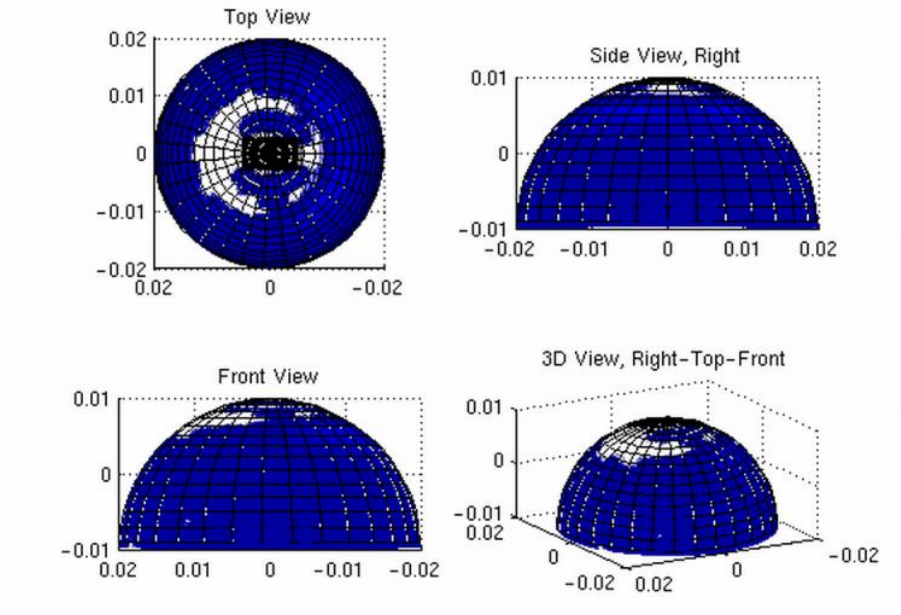

Fig. 5. Concentration of Al particles entering the surrounding; l = 10 mm, θ = 0 degrees, T_o = 300 °C

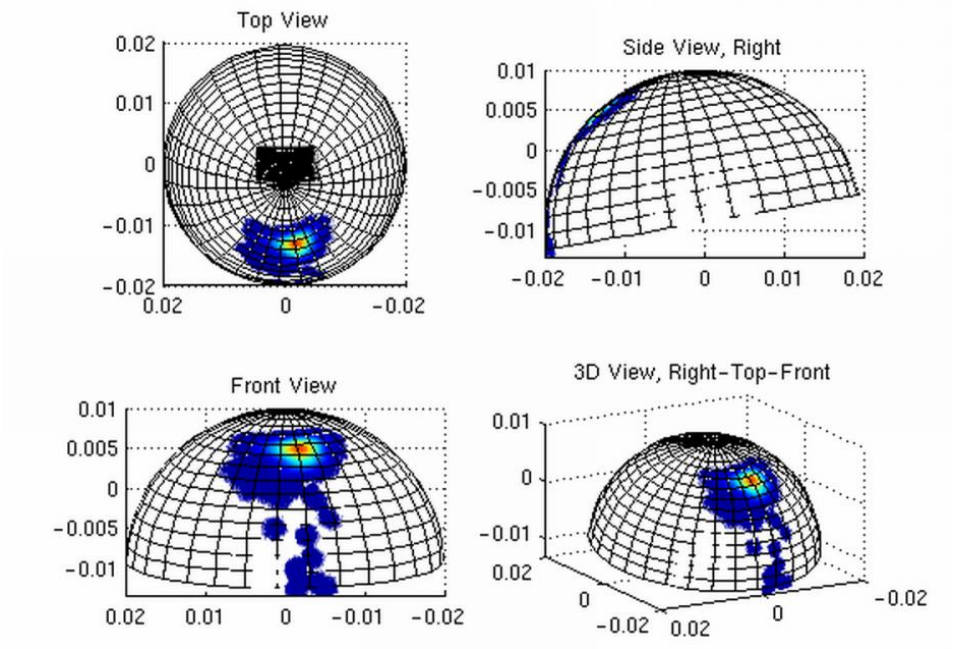

Fig. 6. Concentration of Al particles entering the surrounding; l = 10 mm, θ = 10 degrees, T_o = 300 °C

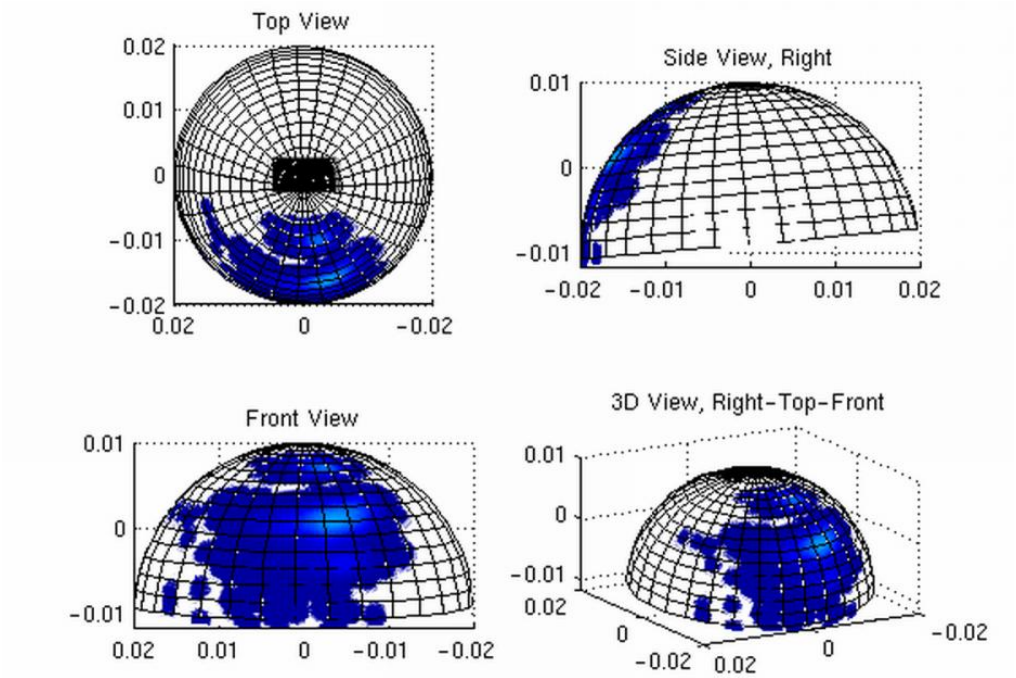

Fig. 7. Concentration of Al particles entering the surrounding; l = 5 mm, θ = 5 degrees, T_o = 300 °C

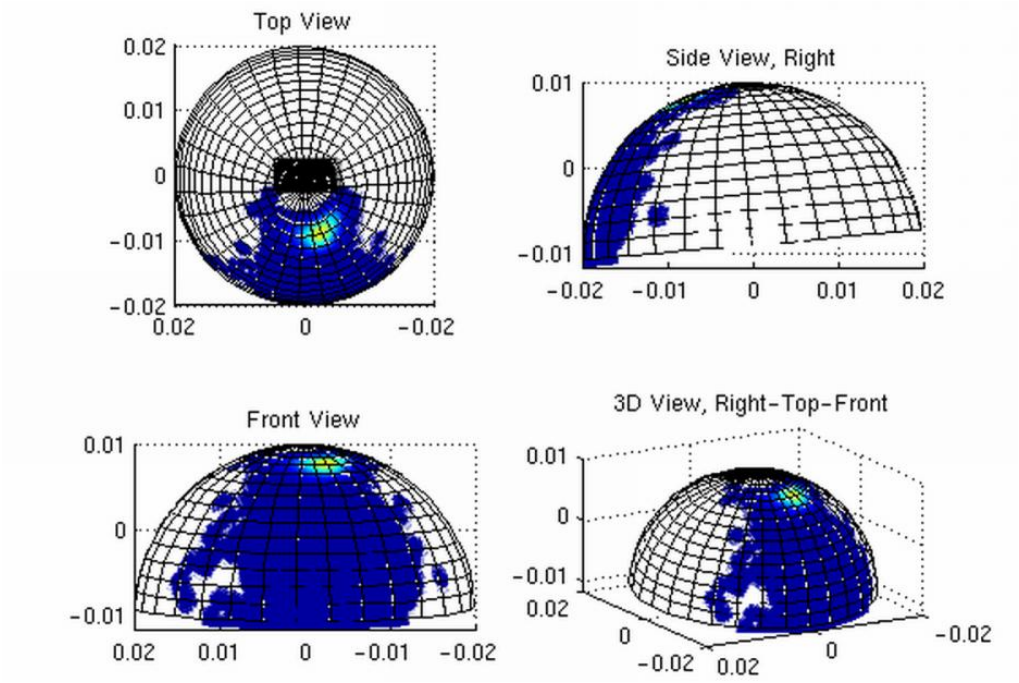

Fig. 8. Concentration of Al particles entering the surrounding; l = 15 mm, θ = 5 degrees, T_o = 300 °C

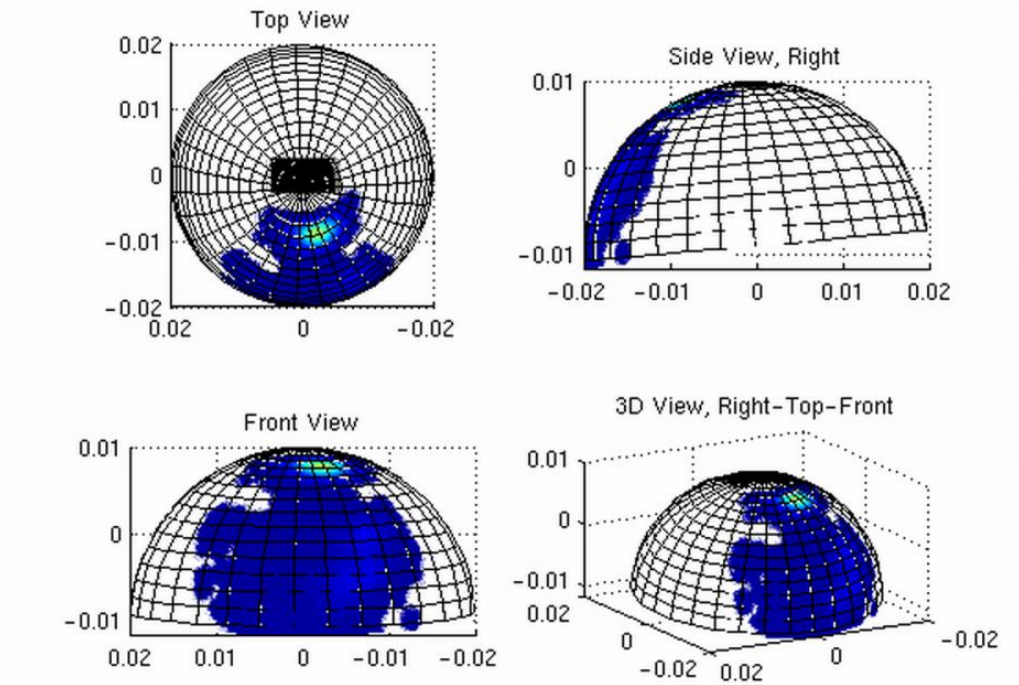

Fig. 9. Concentration of Al particles entering the surrounding; l = 10 mm, θ = 5 degrees, T_o = 100 °C

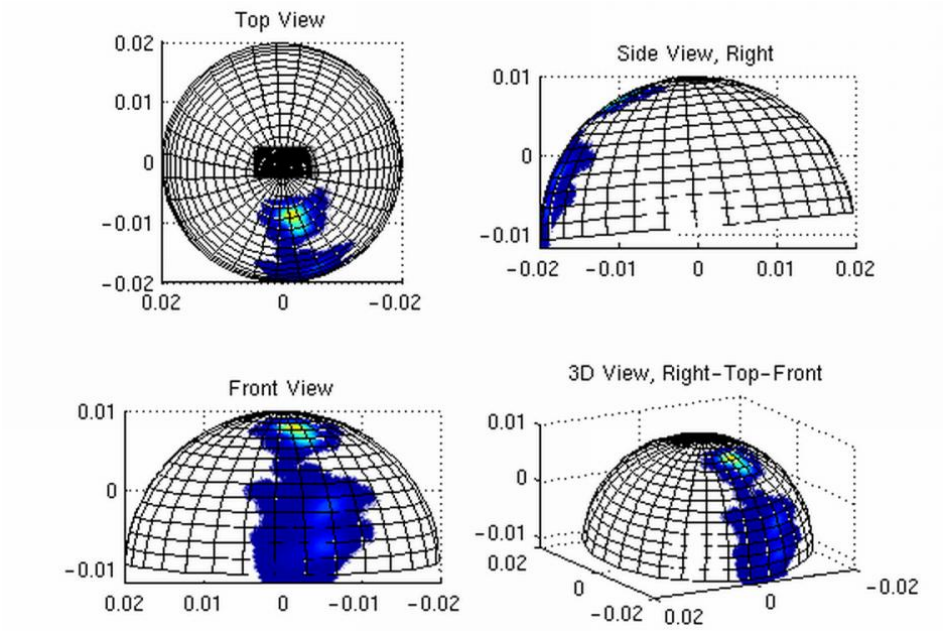

Fig. 10. Concentration of Cu particles entering the surrounding; l = 10 mm, θ = 5 degrees, T_o = 300 °C

3.4 Quantitative Presentation of Results

A quantitative representation of the results is shown in Fig. 11 (a) and (b). The plots are generated for aluminum particles and a spray temperature of 100 °C.

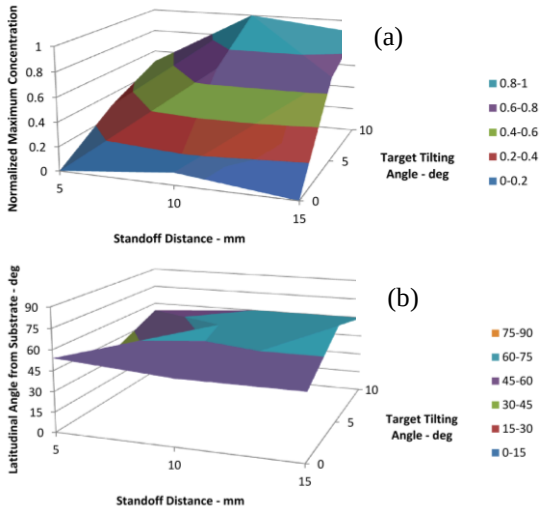

Fig. 11. Quantitative representation of results for aluminum particles and a spray temperature of 100 °C, representing the effect of target tilting angle and standoff distance on (a) normalized maximum particle concentration and (b) latitudinal angle of the spot from substrate, deg.

As seen in previous plots, particle material and spray temperature have insignificant effect on the exhaust pattern, and therefore are not further analyzed in a quantitative fashion. In these plots, for each point the location of the maximum concentration was identified, regardless of the longitudinal location, its normalized magnitude as well as its latitudinal value is recorded. The results show that the most important factor influencing the exhaust pattern is the target tilting angle. In cases of zero-degree angle the particles spread in an approximately equal manner over the environment and exhibit no particular distribution, except for variations due to the asymmetry stemmed from the position of the particle feed. This is reflected in the fact that the normalized maximum concentration value, as depicted in Fig. 11(a), is nearly zero with very slight variations at the target tilting angle of 0 deg. As the tilt angle increases, the location where particles enter the surroundings is more well defined, as the normalized maximum concentration value steadily increases with an increase in target tilting angle.

The different spray parameters have little effect on the location where particles enter the surroundings, as shown in Fig. 11 (b). The value of the latitudinal angle of the point of the highest concentration varies in the range of 45-60. This allows to design the capture-at-source exhaust collection system to be designed to cover this range of the spatial spectrum.

4. CONCLUSION

Computational methods and procedures are successfully used to simulate the trajectories of cold spray particles within the flow field surrounding the substrate. The method is general enough that, as

demonstrated here, can be applied to a range of geometrical and operational parameters of interest. The method that has been developed for post-processing the data offers a convenient tool for drawing comparisons.

The most important factor influencing the exhaust pattern is the target tilting angle. In cases of zero-degree angle the particles spread in an approximately equal manner over the environment and exhibit no particular distribution, except for variations due to the asymmetry stemmed from the position of the particle feed. As the tilt angle increases, the location where particles enter the surroundings becomes more well-defined.

The standoff distance and upstream nozzle temperature have little effect on the location where particles enter the surroundings. Slight behavior differences are observed due to the particle density. Aluminum particles, due to their lower density, are more easily influenced by turbulence than copper particles and tend to follow a more random trajectory, making the pattern created significantly larger

ACKNOWLEDGMENTS

The project was supported by CenterLine (Windsor) Limited (Windsor, Ontario, Canada) and through Discovery Grants from the Natural Sciences and Engineering Research Council of Canada.

REFERENCES

Alkhimov A.P., V.F. Kosareve and A.N. Papyrin (1990). A Method of Cold Gas-Dynamic Spray Deposition, *Dokl. Akad. Nauk SSSR*, 315(5), 1062-1065.

Alkhimov A.P., A.n. Papyrin, V.F. Kosarev, N.I. Nesterovich, and M.M. Shushapanov (1994). "*Gas-Dynamic Spray Method for Applying a Coating,*" U.S. Patent 5,302,414.

Alkhimov A.P., A.N. Papyrin, V.F. Kosarev, N.I. Nesterovich, and M.M. Shushapanov (1995). *Method and Device for Coating*, European Patent 0 484 533 B1.

Assadi H., T. Schmidt, H. Richter, J.-O., Kliemann, K. Binder, F. Gartner, T. Klassen and H. Kreye (2011). On Parameter Selection in Cold Spraying, *J. Therm. Spray. Technol.*, 20, 1161-1176.

Brach R.M. (1988). Impact Dynamics with Applications to Solid Particle Erosion, *Int. J. Impact Eng.*, 7 (1), 37-53.

Clift R., J.R. Grace, and M.E. Weber (1978). *Bubbles, Drops, and Particles* New York, (Academic Press).

Cowley M. (2003), Dusting-Off the Hazards of Powder Coating, *Finishing*, 27(12), 18-21.

Dykhuizen R.C., and M.F. Smith (1998). Gas Dynamic Principles of Cold Spray, *J. Therm. Spray. Technol.*, 7(2), 205-212.

Fluent, Inc. (2011). *Fluent 6.2 User's Guide*, Lebanon, NH, USA.

Gilmore D.L., R.C. Dykhuizen, R.A. Neiser, T.J. Roemer, and M.F. Smith (1999). Particle Velocity and Deposition Efficiency in the Cold Spray Process, *J. Therm. Spray. Technol.*, 8(4), 576-582.

Grujicic M., C. Tong, W.S. DeRosset, and D. Helfritch (2003). Flow Analysis and Nozzle-Shape Optimization for the Cold-Gas Dynamic-Spray Process, *Proc Inst Mech Eng B, J. Eng Manuf.*, 217(11), 1603-1613.

Heriaud-Kraemer H., G. Montavon, S. Hertert, H. Robin, and C. Coddet (2003). Harmful Risks for Workers in Thermal Spraying: A Review Completed by a Survey in French Company, *J. Therm. Spray. Technol.*, 12(4), 542-554.

Jodoin, B. (2002). Cold Spray Nozzle Mach Number Limitation, *J. Therm. Spray. Technol.*, 11(4), 496-507.

Karimi M. (2005). *An Investigation of the Cold Gas Dynamic Supersonic Spray Process Particle/Flow Field*, M.Sc Thesis, University of Windsor, Windsor, Canada.

Karimi M., G.W. Rankin, and A. Fartaj (2005). A Numerical Investigation of the Flowfield of a Supersonic Jet Impinging on a Flat Plate, *Proceedings of the CFD Society of Canada*, St. John's, Newfoundland, Canada.

Karimi M., A. Fartaj, G. Rankin, D. Vanderzwet, W. Birtch, J., Villafuerte (2006). Numerical simulation of the cold gas dynamic spray process, *J. Therm. Spray. Technol.*, 15(4), 518-523.

Karimi M., B. Jodoin, G. Rankin (2011). Shock-Wave-Induced Spraying: Modeling and Physics of a New Spray Process, *J. Therm. Spray. Technol.*, 20(4), 866-881.

Kashirin A.I., Klyuev O.F., and Buzdygar T.V. (2002). *Apparatus for Gas-Dynamic Coating*, U.S. Patent 6,402,050.

Kleis I., and Hussainova I. (1999). Investigation of Particle - Wall Impact Process, *Wear*, 233-235, 168-173.

Konstandopoulos A.G. (2006). Particle Sticking/Rebound Criteria at Oblique Impact, *J. Aerosol Sci.*, 37(3), 292-305.

Kosarev V.F., Klinkov S.V., Alkhimov A.P., and Papyrin A.N. (2003). On Some Aspects of Gas Dynamics of the Cold Spray Process, *J. Therm. Spray. Technol.*, 12(2), 265-281.

Matweb (2012). *Material Properties Data Base*, www.matweb.com, January 2012.

Sarkar S., Erlebacher G., Hussaini M.Y., and Kreiss H.O. (1991). Analysis and Modelling of Dilatational Terms in Compressible Turbulence, *J Fluid Mech*, 227, 473-493.

Sarkar S. and Lakshmanan B. (1991). Application of a Reynolds Stress Turbulence Model to the Compressible Shear Layer, *AIAA Journal*, 29(5), 743-749.

Schmidt T., Gartner F., Assadi H., Kreye H. (2006). Development of a generalized parameter window for cold spray deposition, *Acta Mater.*, 54(3), 729-742.

Shipway P.H., and I.M. Hutchings (1994). Method for Optimizing the Particle Flux in Erosion Testing with a Gas-Blast Apparatus, *Wear*, 174(1-2), 169-175.

Shukla V., G.S. Elliott, and B.H. Kear (2000). Nanopowder Deposition by Supersonic Rectangular Jet Impingement, *J. Therm. Spray. Technol.*, 9(3), 394-398.

Stoltenhoff T., H. Kreye, and H.J. Richter (2002). An Analysis of the Cold Spray Process and Its Coatings, *J. Therm. Spray. Technol.*, 11(4), 542-550.

Tannehill, J.C., D.A., Anderson, R.H., Pletcher (1997). *Computational Fluid Mechanics and Heat Transfer, Second Edition*, Philadelphia PA, USA (Taylor and Francis).

Van Steenkiste H.J., J.R., Smith, and R.E. Teets (2002). Aluminum Coatings Via Kinetic Spray with Relatively Large Powder Particles, *Surf. Coat. Technol.*, 154(2-3), 237-252.

Walter J. (1995). Particle-Surface Interactions: Charge Transfer, Energy Loss, Resuspension, and Deagglomeration, *Aerosol Sci. Technol.*, 23(1), 2-24.